Available online at www.sciencedirect.com
SCIENCE DIRECT®
Journal of Catalysis 222 (2004) 180–191
JOURNAL OF CATALYSIS
www.elsevier.com/locate/jcat

Aqueous-phase reforming of oxygenated hydrocarbons over Sn-modified Ni catalysts

J.W. Shabaker, G.W. Huber, and J.A. Dumesic *

Department of Chemical and Biological Engineering, University of Wisconsin, Madison, WI 53706, USA

Received 21 July 2003; revised 22 October 2003; accepted 28 October 2003

Abstract

Reaction kinetics measurements were conducted for aqueous-phase reforming of oxygenated hydrocarbons over Pt/Al_2O_3, Ni/Al_2O_3, $NiSn/Al_2O_3$, Raney-Ni, and Raney-NiSn catalysts at temperatures of 498 and 538 K. Raney-Ni, Raney-NiSn, and Pt/Al_2O_3 catalysts display good stability with time on stream during aqueous-phase reforming, whereas Al_2O_3-supported Ni and NiSn catalysts exhibit deactivation caused by sintering. Aqueous-phase reforming of sorbitol, glycerol, and ethylene glycol solutions produces an effluent gas stream composed of 50–70 mol% H_2, 30–40 mol% CO_2, and 2–11 mol% alkanes (dry basis) at high conversion. Addition of Sn to Ni improves the selectivity for production of H_2 by ethylene glycol reforming from 35 to 51% at a Ni:Sn ratio of 270:1, while the alkane selectivity is reduced from 44 to 33%. At a Ni:Sn ratio of 14:1, the hydrogen selectivity increases to 90%, while alkane production is nearly eliminated. As the system pressure decreases to the bubble point of the feed (25.1 bar at 498 K), production of alkanes decreases and the hydrogen selectivity increases accordingly. Hydrogen selectivity is also maximized by operation at higher reactor space velocities. The addition of Sn to Ni significantly decreases the rate of methane formation from C–O bond cleavage, while maintaining sufficiently high rates of C–C bond cleavage required for hydrogen formation. Turnover frequencies for hydrogen production at 498 K over Raney-Ni-based catalysts are several times lower than that over 3 wt% Pt/Al_2O_3 based on CO chemisorption. However, the high CO uptakes and high densities of Raney-Ni-based catalysts lead to comparable rates of hydrogen production per unit reactor volume as 3 wt% Pt/Al_2O_3 at 498 K. Results from XRD, SEM, and ^{119}Sn Mössbauer spectroscopy suggest that Raney-NiSn catalysts comprise alumina and nickel particles surrounded by a Ni–Sn alloy. After exposure to reaction conditions, Sn is present primarily as Ni_3Sn alloy with small amounts of Sn(IV) probably associated with alumina.

Keywords: Ethylene glycol; Glycerol; Sorbitol; Reforming; Hydrogen production; Nickel tin catalysts

1. Introduction

Extensive research is being conducted worldwide to develop hydrogen fuel cells for environmentally benign generation of energy, since these devices operate at high efficiencies and water is the only by-product formed during operation. However, production of hydrogen fuel for these devices is currently limited to energy-intensive processing of nonrenewable hydrocarbons, such as steam reforming of natural gas. The full environmental benefits of using hydrogen as a fuel are realized when hydrogen is derived from renewable sources. In this respect, we have recently reported a process to generate hydrogen by aqueous-phase reforming (APR) at temperatures near 500 K of oxygenated hydrocarbons derived from biomass, such as sorbitol, glycerol, and ethylene glycol [1–4]. In addition to utilizing renewable feedstocks, the APR process eliminates the need to vaporize water and the oxygenated hydrocarbon, which reduces the energy requirements for producing hydrogen and leads to low levels of CO (< 1000 ppm) in a single-step catalytic process. Effluent CO concentrations can be reduced below 100 ppm using a second reactor [5]. Another advantage of the APR process is that it is greenhouse gas neutral, because the CO_2 by-product that accompanies the H_2 is consumed by biomass growth.

Aqueous-phase reforming of oxygenated hydrocarbons, such as methanol and ethylene glycol, takes place according to the following stoichiometric reactions:

$$CH_3OH + H_2O \rightarrow 3H_2 + CO_2, \quad (1)$$

$$C_2H_6O_2 + 2H_2O \rightarrow 5H_2 + 2CO_2. \quad (2)$$

* Corresponding author.
E-mail address: dumesic@engr.wisc.edu (J.A. Dumesic).

0021-9517/$ – see front matter
doi:10.1016/j.jcat.2003.10.022

These reactions may take place via formation of CO as an intermediate product, which is subsequently converted to CO_2 by the water–gas-shift reaction:

$$CO + H_2O \leftrightarrow H_2 + CO_2. \quad (3)$$

Generation of H_2 and CO_2 by liquid-phase reforming at low temperatures, however, is accompanied by selectivity challenges, since the reaction of H_2 with CO or CO_2 to form alkanes (C_nH_{2n+2}) is highly favorable at these low temperatures. For example, the equilibrium constant at 500 K for the conversion of CO_2 and H_2 to give methane by the following reaction is of the order of 10^{10} per mole of CO_2.

$$CO_2 + 4H_2 \leftrightarrow CH_4 + 2H_2O. \quad (4)$$

Thus an effective catalyst for production of H_2 by aqueous-phase reforming of oxygenated hydrocarbons must break C–C, O–H, and C–H bonds in the oxygenated hydrocarbon reactant, and the catalyst must facilitate a water–gas shift to remove adsorbed CO from the surface. However, the catalyst must neither cleave C–O bonds nor hydrogenate CO or CO_2 to form alkanes.

We have previously reported that silica-supported Pt and Pd are selective for production of H_2 from aqueous-phase reforming of ethylene glycol, with Pt/SiO_2 being more active [2]. Silica-supported Ni and Ru are active for aqueous-phase reforming of ethylene glycol, but these metals produce undesired alkanes [2]. In contrast, silica-supported Rh and Ir show low activity for aqueous-phase reforming of ethylene glycol [2]. We also showed in later studies that alumina is an effective support for aqueous-phase reforming catalysts [4].

We have recently reported that addition of Sn to Ni catalysts decreases the rate of formation of alkanes by aqueous-phase reforming without changing the rate of hydrogen production [6]. In particular, we have developed a Raney Ni–Sn catalyst that has comparable activity and selectivity for production of H_2 as Pt/Al_2O_3 [1]. In the present paper, we report results from catalyst characterization studies and reaction kinetics measurements for aqueous-phase reforming over Pt/Al_2O_3, Ni/Al_2O_3, $NiSn/Al_2O_3$, Raney-Ni, and Raney-NiSn catalysts. The results from these studies allow us to document the role of Sn in controlling the selectivity of Ni-based catalysts and to determine the reaction conditions under which NiSn-based catalysts perform as well or better than Pt/Al_2O_3 catalysts for aqueous-phase reforming reactions.

2. Experimental

2.1. Catalyst preparation

Alumina-supported Ni and Pt catalysts were prepared by incipient wetness impregnation of the support (Catapal B, Grace) with aqueous solutions of nickel nitrate hexahydrate ($Ni(NO_3)_2 \cdot 6H_2O$, Aldrich), and tetraamine platinum nitrate ($Pt(NH_3)_4(NO_3)_2$, Strem), respectively, followed by drying in air at 393 K for 12 h. The Ni/Al_2O_3 and Pt/Al_2O_3 catalysts were subsequently calcined for 2 h in a Pyrex cell in 10% O_2/He (300 cm^3(STP) min^{-1}) at 533 K (heating at 1.3 K min^{-1}). A Ni_9Sn/Al_2O_3 catalyst was prepared by incipient wetness impregnation of the dried, uncalcined Ni/Al_2O_3 catalyst with a solution of tributyl tin acetate ($(C_4H_9)_3SnCH_3COO$, Aldrich) in ethanol, followed by drying at 393 K for 12 h. Prior to use, the Pt/Al_2O_3 catalyst was reduced for 2 h at 533 K (heated at 1 K min^{-1}), while the Ni/Al_2O_3 and Ni_9Sn/Al_2O_3 catalysts were reduced at 723 K.

Raney Ni–Sn (R-Ni_xSn) catalysts were prepared by reducing Raney Ni 2800 (R–Ni) (Grace Davison) at 533 K for 2 h (heating at 0.5 K min^{-1}) in flowing H_2, adding appropriate amounts of a 9.4 wt% Sn (tributyl tin acetate) solution in ethanol to reduced R-Ni under a N_2 atmosphere, and subsequently heating the mixture in a sealed Parr acid digestion bomb to 423 K for 2 h (heating at 0.5 K min^{-1}). Prior to catalyst characterization or collecting reaction kinetics data, all catalysts were reduced in flowing H_2 (100 cm^3(STP) min^{-1}) for 2 h at 533 K (heating at 0.5 K min^{-1}). Catalysts were passivated for ex situ studies by loading each reduced catalyst in a closed vial in a glove box followed by exposing the closed vial to the atmosphere for 24 h.

2.2. High-throughput studies

A high-throughput 48-well, stainless-steel batch reactor system was developed to screen catalysts for aqueous-phase reforming of oxygenated hydrocarbons. Catalyst samples were tested in parallel by loading them into separate 1-cm^3 wells. The catalysts in the 48-well system were reduced in flowing H_2 (e.g., at 530 K) under a common head space and then purged with He to remove the H_2. After cooling to room temperature, aqueous solutions of 2 wt% ethylene glycol were pipetted into each well under a He atmosphere in a glove box. The wells were then sealed with a high temperature silicone rubber gasket and a stainless-steel cover plate with 1.6 mm (1/16 inch) holes for each well. The 48-well system was subsequently heated for 7.5 h at 473 K and then cooled to room temperature. The gas-phase product of each well was sampled by inserting a syringe through the holes in the cover plate, and the gas was injected into a GC to determine the amounts of H_2 and CH_4 present in each well. The liquid phase of each well was analyzed by thin-layer chromatography (TLC) coupled with a scanner and Scion Image software to determine the conversion of ethylene glycol.

2.3. Reaction kinetics measurements

Reaction kinetics measurements were performed using a reactor system described elsewhere [3]. Alumina-supported catalyst samples were sieved to −120 mesh size (particle diameters less than 63 μm) to alleviate transport limitations for kinetics runs and pelletized for low pressure drop (less

than 1 bar) during high conversion runs [3]. The Raney catalysts were loaded without sieving (particle diameters are 45–90 μm) or pelletizing. Aqueous solutions containing 1 or 5 wt% oxygenate were fed to the reactor at flow rates between 0.06 and 0.40 $cm^3\,min^{-1}$ (LHSV of 0.82–130 h^{-1}). Reaction kinetics measurements were made at temperatures of 498 and 538 K and system pressures between 25.8 and 51.3 bar, at least 0.5 bar above the bubble point of the feed solution. Each reaction condition was maintained for at least 6 h to assure that steady state had been achieved, as determined by online gas chromatography. The liquid-phase effluent from the reactor was collected during reaction kinetics measurements, and this liquid was analyzed via gas chromatography (FID detector), high-performance liquid chromatography (HPLC, RI and UV detectors), and total organic carbon (TOC) measurements.

2.4. Catalyst characterization studies

Mössbauer spectra were collected with an Austin Science Associates Model S-600 Mössbauer spectrometer operated in constant-acceleration mode with a 20 mCi γ-ray $Ca^{119}SnO$ source. A 0.05-mm-thick Pd foil was placed between the source and the detector to filter 25.04- and 25.27-keV X-rays from the source. A Xe–CO_2 proportional counter was used for detection of the 23.88 keV γ-rays. Isomer shifts are reported relative to $CaSnO_3$ at room temperature. A thin-window glass cell was used for treatments and to collect Mössbauer data. Spectra were also collected after exposure to reaction conditions, in which the spent catalyst sample was transferred from the sealed reaction vessel to the Mössbauer cell under a He atmosphere in a glove box.

X-ray diffraction (XRD) data were collected with a Cu-K_α source using a Scintag PADV diffractometer operating at 40.0 mA and 35.0 kV. The pattern was collected in continuous-scan mode with steps of 0.3° min^{-1}. The Scherrer equation was used to estimate the Ni crystal size. Scanning electron microscope (SEM) images were collected on a LEO DSM 1530 field emission scanning electron microscope equipped with an energy-dispersive analysis system (EDS/EDX) with a resolution of 129 eV at Mn.

Raney-Ni and -NiSn catalysts were analyzed by X-ray photoelectron spectroscopy (XPS) after passivation in air on a Perkin-Elmer 5400 ESCA spectrometer with an Al source operating at 15 kV and 300 W. The surface concentrations were measured using the Ni $2p^3$, O 1s, and Sn $3d^5$ peak areas and sensitivities published elsewhere [7]. The number of surface Ni or Pt atoms on each catalyst was determined from the irreversible chemisorption of CO and total chemisorption uptake of H_2 at 298 K, as described elsewhere [2]. BET surface areas of the Raney catalysts were found by N_2 adsorption at 77 K. Metal loadings on catalysts were determined by atomic absorption spectroscopy (AAS/ICP).

3. Results

3.1. High-throughput studies

More than 300 catalysts were screened for aqueous-phase reforming of ethylene glycol in the high-throughput reactor, including supported monometallic, supported bimetallic, and skeletal Ni-based catalysts. High-throughput studies of Ni supported on ZrO_2, activated carbon, TiO_2, and Al_2O_3 showed that Ni catalysts supported on ZrO_2, TiO_2, and Al_2O_3 were more active than Ni catalysts supported on carbon, while the selectivity for H_2 production increased in the order TiO_2 < carbon < ZrO_2 < Al_2O_3. These results for supported Ni catalysts follow trends similar to those exhibited by Pt supported on the same materials [4].

High-throughput studies of Al_2O_3-supported Ni catalysts showed that addition of Sn, Au, or Zn improved the hydrogen selectivity of the catalyst, with Ni–Sn/Al_2O_3 catalysts being the most active and selective. However, as will be shown later, Ni–Sn/Al_2O_3 catalysts were not stable with respect to time on stream during aqueous-phase reforming, so a method of adding Sn to Raney-Ni was developed. Over these Raney-NiSn catalysts, addition of Sn caused a decrease in the rate of methane production while the rate of H_2 production did not change significantly, as shown in Fig. 1. For example, addition of only 0.5 wt% Sn (Ni:Sn atomic ratio of 400:1) reduces the rate of methane production by about one-half, while the rate of hydrogen production increases slightly. Methane production is nearly eliminated by addition of more than 10 wt% Sn (Ni:Sn atomic ratio of 18:1), while the rate of hydrogen production is decreased only slightly. Carbon conversion decreases with addition of Sn because the rate of methane production decreases. Similar trends were observed for NiSn/Al_2O_3 catalysts with a range of Ni:Sn ratios and reduced at 723 K. The R-$Ni_{14}Sn$ and Ni_9Sn/Al_2O_3 catalysts had the minimum Sn content necessary to minimize methane formation and maximize hydrogen production.

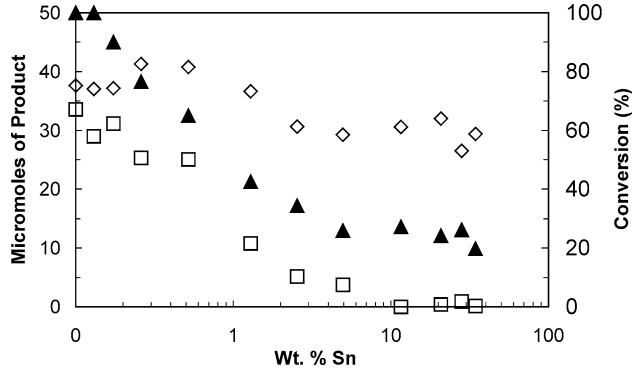

Fig. 1. Results of catalyst screening showing effect of Sn addition to Raney 2800 for production of H_2 (◇), CH_4 (■), and conversion (%) (▲) for aqueous reforming of 2 wt% ethylene glycol solutions in the high-throughput, parallel batch reactor. Each point is average of three replicate wells containing the same amount of each catalyst.

Table 1
Characterization of catalysts

Catalyst	Sn[a] (wt%)	Sn/Ni bulk atomic ratio[b]	Irreversible CO uptake (μmol g^{-1})	Irreversible H_2 uptake (μmol g^{-1})	BET surface area (m^2 g^{-1})	CO/Ni or CO/Pt atomic ratio	CO/H uptake ratio	Ni particle size[c] (nm)
Raney Ni 2800	0	0	222	153	46.6	0.014	0.73	38
Raney $Ni_{270}Sn$	0.69	0.004	205	134	53.2	0.013	0.76	38
Raney $Ni_{14}Sn$	12.4	0.07	169	20.4	46.6	0.012	4.14	38
Raney $Ni_{14}Sn$ after reaction	12.4	0.07	140	47.6	48.8	0.010	1.47	40
Raney Ni_4Sn	31	0.23	57.1	10.2	31.9	0.0034	2.80	38
14.8% Ni/Al_2O_3[d]	0	0	147	–	–	0.058	–	< 10
14.8% Ni_9Sn/Al_2O_3[d]	3.3	0.11	168	–	–	0.067	–	< 10
14.8% Ni_9Sn/Al_2O_3 13.5% Ni after reaction[d]	3.4	0.13	8.9	–	–	0.0040	–	38
3.4% Pt/Al_2O_3	0	0	106	72	–	0.60	0.74	–

[a] Determined by ICP.
[b] Determined by ICP.
[c] Determined by XRD.
[d] Reduced at 723 K, percentage is Ni loading only.

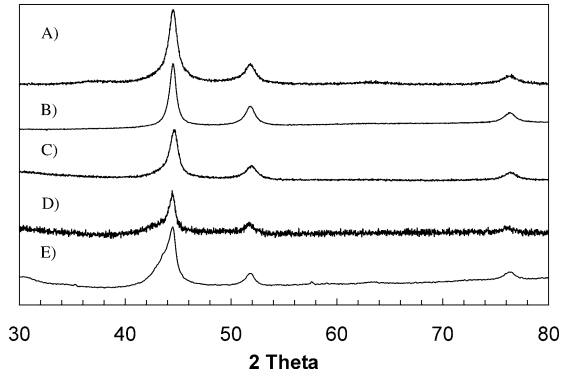

Fig. 2. X-ray diffraction patterns of passivated samples: (A) Raney Ni 2800 reduced at 533 K, (B) Raney $Ni_{270}Sn$ reduced at 533 K, (C) Raney $Ni_{14}Sn$ reduced at 533 K, (D) Raney $Ni_{14}Sn$ after reaction at 498 K, and (E) Raney Ni_4Sn reduced at 533 K.

3.2. Catalyst characterization studies

Characteristics of the catalysts used in this study are summarized in Table 1. Addition of Sn to R-Ni and subsequent exposure of the catalyst to reaction conditions had little effect on the X-ray diffraction pattern of the catalyst, as shown in Fig. 2. All XRD peaks observed for the reduced R-Ni, R-$Ni_{270}Sn$, and R-$Ni_{14}Sn$ catalysts were metallic Ni, including the R-$Ni_{14}Sn$ catalyst after exposure to reaction conditions at 498 K for 60 h. The R-Ni_4Sn catalyst showed similar peaks due to metallic Ni as the other Raney catalysts, as well as a shoulder near $2\theta = 44°$ that is characteristic of Ni–Sn alloys. The XRD peak widths were similar for all R-Ni-based catalysts, indicating that the Ni particle sizes (estimated to be ~ 40 nm from the Scherrer equation) were comparable.

Low-magnification scanning electron micrographs of R-Ni and R-$Ni_{14}Sn$ showed typical granular characteristics of Raney catalysts. High-magnification micrographs of the R-Ni catalyst (Fig. 3) show a predominant porous region and a less-extensive solid phase distributed on top of the porous region. X-ray microanalyses of these regions indicate that the porous region is Ni rich and the other region is rich in Al and O. In agreement with previous electron microscopy and electron diffraction studies, these results in-

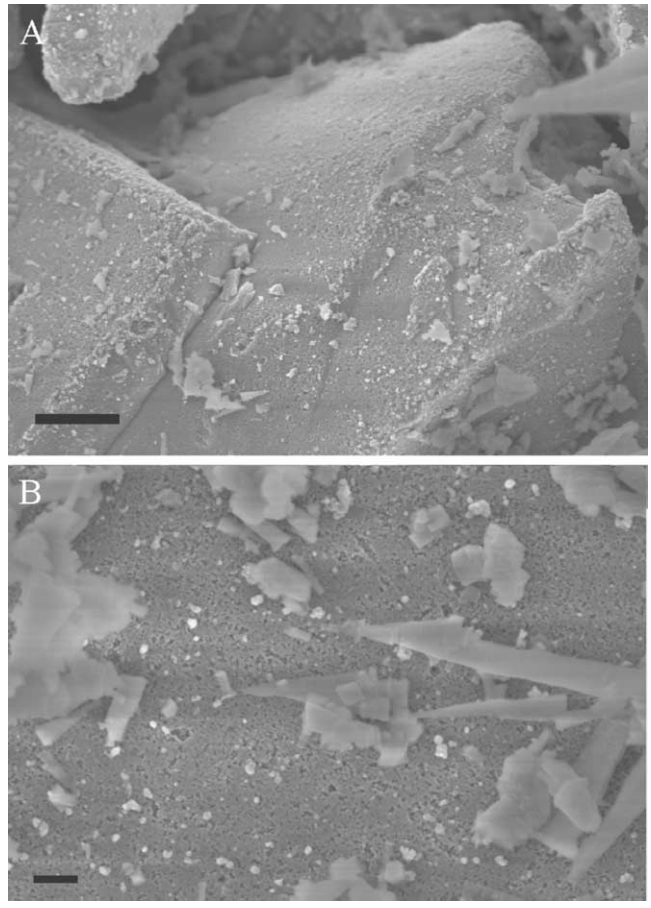

Fig. 3. SEM micrographs of a fresh R-Ni catalyst reduced at 533 K shown at (A) low magnification (scale bar is 1 μm) and (B) high magnification (scale bar is 200 nm).

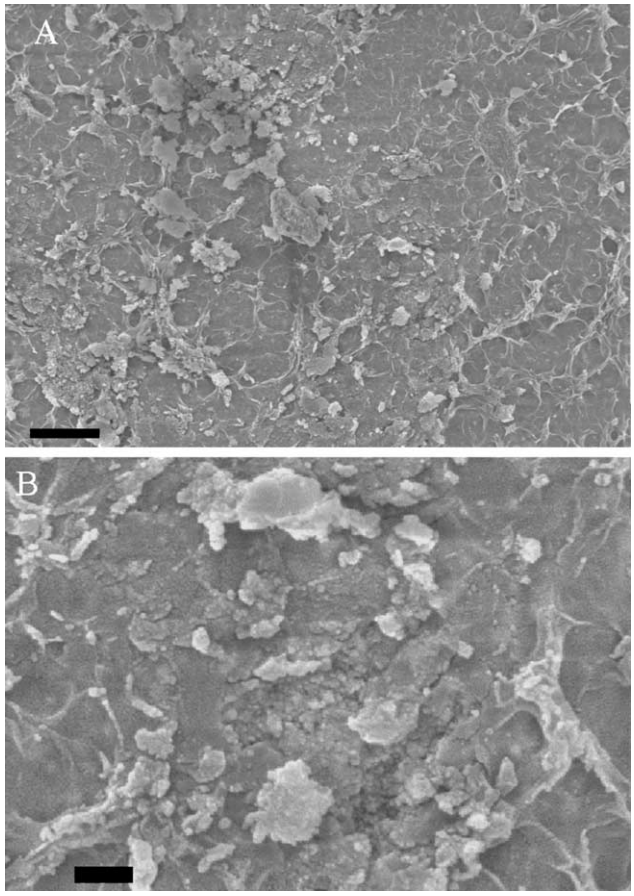

Fig. 4. SEM micrographs of a fresh R-$Ni_{14}Sn$ catalyst reduced at 533 K shown at (A) low magnification (scale bar is 1 μm) and (B) high magnification (scale bar is 200 nm).

dicate that R-Ni catalysts are porous Ni frameworks covered by hydrated alumina particles [8]. The R-$Ni_{14}Sn$ catalyst (Fig. 4) also appears to have a predominant porous region and a diffuse phase covering parts of the porous region, but X-ray microanalyses could not differentiate between these two phases.

Fig. 5 shows R-$Ni_{14}Sn$ after reaction at 498 K, in which the diffuse phase disappears and two separate phases are seen: porous Ni-rich regions (Fig. 5A) and crystalline regions containing primarily Al and O (Fig. 5B). Both of these regions contain Sn. Thus, the aluminum-rich phase forms crystallites (100–700 nm long, see inset) after exposure to aqueous-phase reforming reaction conditions, while the porous Ni-rich region remains intact.

In situ ^{119}Sn Mössbauer spectroscopy was used to determine the chemical environment of the Sn species in the Ni–Sn catalysts. Spectra of the alumina-supported catalyst are shown in Fig. 6, and parameters derived from fitting these spectra are listed in Table 2. After reduction at 723 K, the Ni_9Sn/Al_2O_3 catalyst contained a mixture of Ni_3Sn alloy and Sn(0) phases, with a small amount of Sn(II) that may be associated with the alumina support. While few Mössbauer spectroscopic studies of Ni_3Sn alloys are available, the isomer shift (IS) of the Ni_3Sn alloy can be inferred from studies of Ni_3Sn_2 (IS = 1.73 mm s^{-1}) and Ni_3Sn_4 (IS = 1.97 mm s^{-1}), because this parameter generally increases linearly with increasing atomic fraction of Sn in the alloy [9].

Exposure of the reduced Ni_9Sn/Al_2O_3 catalyst to reaction conditions and re-reduction converted nearly all of the Sn(0) to Ni_3Sn alloy. Thus, under reaction conditions, Sn migrates

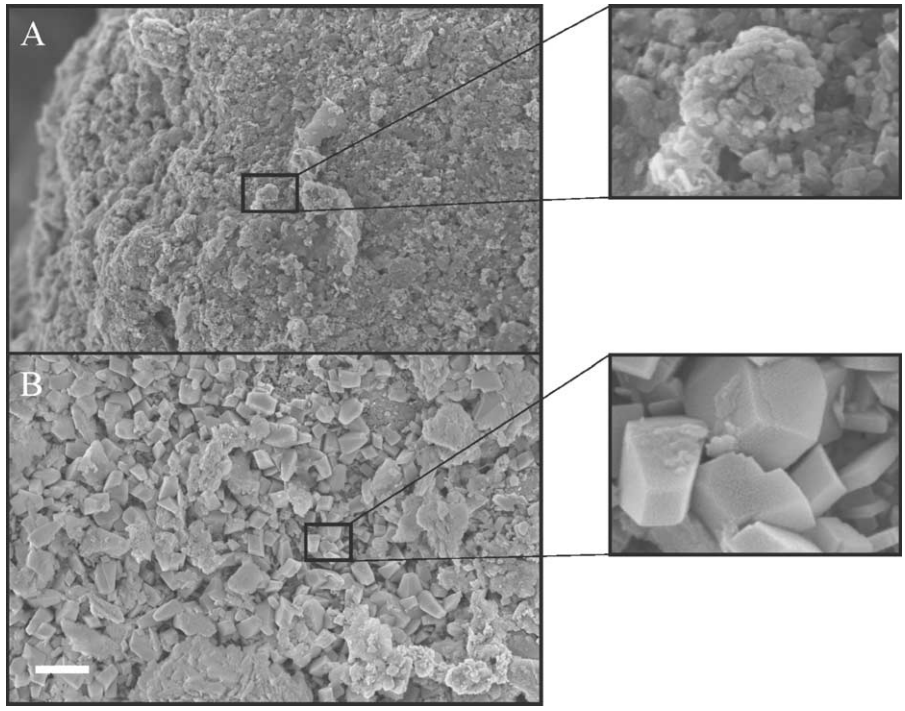

Fig. 5. SEM micrographs of spent R-$Ni_{14}Sn$ catalyst after reaction at 498 K for 60 h: (A) Ni-rich region and (B) Al-rich region. Large panels are low magnification (scale bar is 1 μm), inset images are magnified 6× further.

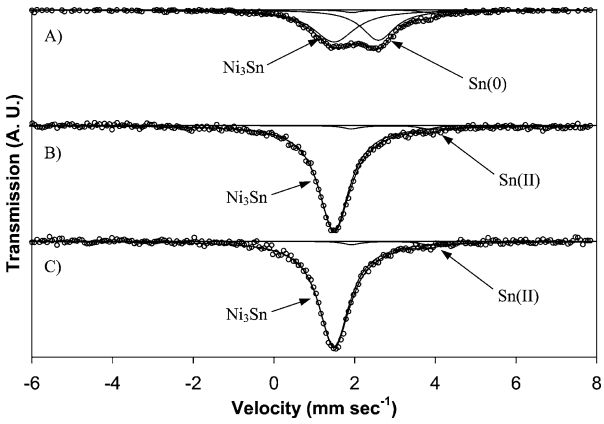

Fig. 6. In situ ^{119}Sn Mössbauer spectra of Ni_9Sn/Al_2O_3 after (A) reduction at 723 K, (B) reaction, passivation, and re-reduction at 723 K, and (C) reaction, re-reduction at 723 K, and passivation.

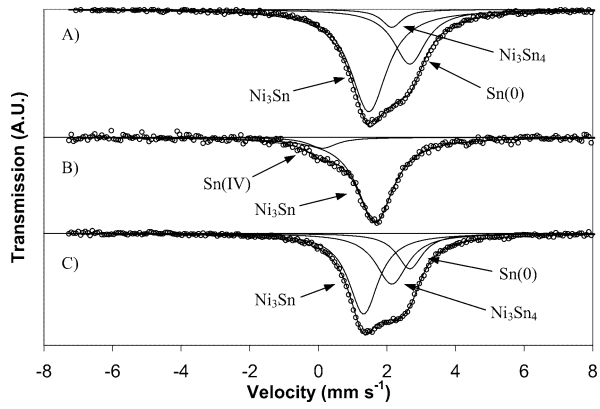

Fig. 7. In situ ^{119}Sn Mössbauer spectra of (A) Raney $Ni_{14}Sn$ after reduction at 533 K, (B) Raney $Ni_{14}Sn$ after reaction at 498 K and 25.8 bar with 5 wt% ethylene glycol solution, and (C) Raney Ni_4Sn after reduction at 533 K.

Table 2
^{119}Sn Mössbauer parameters at 300 K for catalyst samples

Sample and treatment	IS ($mm\,s^{-1}$)	QS ($mm\,s^{-1}$)	Width	Relative area (%)	Chemical form of Sn
Ni_9Sn/Al_2O_3	1.49	0.00	1.26	55.2	Ni_3Sn
Reduced at 723 K	2.87	1.89	0.54	3.9	Sn(II)
	2.59	0.00	0.98	41.0	Sn(0)
Ni_9Sn/Al_2O_3	1.49	0.00	0.93	94.0	Ni_3Sn
After reaction,	2.87	1.89	0.52	3.3	Sn(II)
re-reduced at 723 K	2.48	0.00	1.00	2.8	Sn(0)
Ni_9Sn/Al_2O_3	1.49	0.00	0.93	94.0	Ni_3Sn
After reaction,	2.87	1.89	0.52	3.3	Sn(II)
re-reduced at 723 K, and passivation	2.48	0.00	1.00	2.8	Sn(0)
Raney $Ni_{14}Sn$	1.47	0.00	1.29	63.6	Ni_3Sn
Reduced at 533 K	2.67	0.00	1.14	30.1	Sn(0)
	2.14	0.00	0.71	6.3	Ni_3Sn_4
Raney $Ni_{14}Sn$	1.66	0.00	1.27	90.7	Ni_3Sn
After reaction	0.12	0.00	1.01	9.3	Sn(IV)
Raney Ni_4Sn	1.32	0.00	1.05	48.7	Ni_3Sn
Reduced at 533 K	2.66	0.00	0.90	18.4	Sn(0)
	2.14	0.00	1.14	32.9	Ni_3Sn_4

into Ni particles to form the alloy. Subsequent exposure to air had no effect on the state of the Sn in the catalyst. This observation is consistent with the results presented below which indicate that the Ni_3Sn alloy particles on alumina are poorly dispersed after exposure to aqueous-phase reforming reaction conditions.

Mössbauer spectra of the Raney Ni–Sn catalysts are shown in Fig. 7. The reduced R-$Ni_{14}Sn$ catalyst contains Sn in three states (Fig. 7A): Ni_3Sn, Ni_3Sn_4 and metallic Sn, with relative spectral areas of 64, 6, and 30%, respectively. After exposure to reaction conditions (Fig. 7B), the peaks caused by metallic Sn and Ni_3Sn_4 disappear, accompanied by the appearance of a small peak related to Sn(IV). The relative areas of the Ni_3Sn and Sn(IV) peaks are 90 and 10%, respectively. In view of the SEM results, it is probable that the Sn(IV) peak is associated with crystalline alumina. The Ni_3Sn alloy phase probably surrounds a phase that is Ni rich (seen in XRD), since the Ni–Sn phase diagram predicts a mixture of Ni_3Sn and Ni for all our NiSn catalysts [10]. After reduction, the R-Ni_4Sn catalyst contains smaller relative amounts of Sn(0) and Ni_3Sn than the R-$Ni_{14}Sn$ catalyst and larger amounts of the Ni_3Sn_4 phase (Fig. 7C).

Characterization of a Sn-promoted Raney-Ni catalyst by X-ray photoelectron spectroscopy showed that tin does not disappear from the surface by complete dissolution into the bulk Ni particles. The surface Sn/Ni atomic ratio measured by XPS on the passivated R-$Ni_{14}Sn$ catalyst was equal to 0.05 before reaction and 0.02 after reaction, and both of these values are slightly lower but comparable to the bulk Sn/Ni atomic ratio of 0.07. Similarly, the surface Sn/Ni atomic ratio of the R-Ni_4Sn catalyst was 0.23, very similar to its bulk atomic ratio.

The addition of Sn to the R-Ni catalyst decreases the extent of CO adsorption. Specifically, the irreversible extent of CO chemisorption decreased from 222 $\mu mol\,g^{-1}$ for R-Ni to 205, 169, and 57.1 $\mu mol\,g^{-1}$ for R-$Ni_{270}Sn$, R-$Ni_{14}Sn$, and R-Ni_4Sn, respectively (Table 1). The CO uptake decreased from 169 to 140 $\mu mol\,g^{-1}$ after exposure of the R-$Ni_{14}Sn$ catalyst to aqueous-phase reforming reaction conditions (498 K and 25.8 bar) for 60 h, passivation, and re-reduction. The CO uptakes of the $NiSn/Al_2O_3$ catalyst decreased dramatically after exposure to reaction conditions, from CO/Ni ratios near 0.06 to 0.004. This significant decrease in the CO uptake is caused by sintering of the Ni–Sn alloy particles on alumina, as evidenced by narrowing of the X-ray diffraction peaks.

The addition of Sn to R-Ni causes the hydrogen adsorption uptake to decrease more dramatically than the CO adsorption uptake. For example, the extent of H_2 adsorption decreased from 153 $\mu mol\ H_2\,g^{-1}$ for R-Ni to 134, 20.4, and 10.2 $\mu mol\ H_2\,g^{-1}$ for R-$Ni_{270}Sn$, R-$Ni_{14}Sn$, and R-Ni_4Sn, respectively. Accordingly, the surface CO:H ratio calculated from the irreversible CO and H_2 uptakes increases from 0.73 for R-Ni (near the typical value of 0.7 for Ni surfaces [11]) to

Table 3
Experimental data for reforming of aqueous 1 wt% ethylene glycol, glycerol, and sorbitol solutions over R-$Ni_{14}Sn$ (1) and 3 wt% Pt/Al_2O_3 (2) catalysts[a]

	Feed molecule											
	Sorbitol				Glycerol				Ethylene glycol			
Temperature (K)	498		538		498		538		498		538	
Catalyst	NiSn	Pt	NiSn	Pt	NiSn	Pt	NiSn	Pt	NiSn	Pt	NiSn	Pt
Pressure (bar)	25.8	29.3	51.4	56.0	25.8	29.3	51.4	56.0	25.8	29.3	51.4	56.0
LHSV (h^{-1})	1.64	0.64	1.64	0.64	1.64	0.64	10.3	0.64	5.14	0.64	12.9	0.64
% Carbon in liquid-phase effluent	44	39	9	12	13	17	4	3	2	11	0	3
% Carbon in gas-phase effluent	55	61	90	90	86	83	100	99	93	90	100	99
Gas-phase composition (mol%)												
H_2	59	61	52	54	66	65	64	57	70	70	70	69
CO_2	34	35	36	36	30	30	30	32	28	29	28	29
Methane	6.1	2.5	8.2	6.0	4.5	4.2	5.8	8.3	1.3	0.8	2.0	2.0
Ethane	0.8	0.7	2.1	2.3	0.0	0.9	0.1	2.0	0.0	0.1	0.0	0.3
Propane	0.1	0.8	0.8	1.0	0.0	0.4	0.0	0.7	0.0	0.0	0.0	0.0
C_4, C_5, C_6 alkanes	0.0	0.0	0.4	0.6	0.0	0.0	0.0	0.0	0.0	0.0	0.0	0.0
H_2 selectivity (%)	65	66	46	46	81	75	76	51	95	96	95	88
Alkane selectivity (%)	19	15	31	32	13	19	17	31	4	4	7	8

[a] H_2 selectivity (%) is calculated as (molecules H_2 produced/C atoms in gas phase)(1/RR) ×100, where RR is the H_2/CO_2 reforming ratio, which depends on the reactant compound. RR values for the compounds are sorbitol, 13/6; glycerol, 7/3; ethylene glycol, 5/2. We note that H_2 and alkane selectivies do not add up to 100% because they are based on independent H balances and C balances, respectively. % Alkane selectivity is calculated as (C atoms in gaseous alkanes)/(total C atoms in gas-phase product) ×100. The liquid hourly space velocity (LHSV, h^{-1}) is defined as (volumetric flow rate of feed solution ($cm^3\,h^{-1}$))/(catalyst bed volume (cm^3)). The weight hourly space velocity (WHSV, h^{-1}) may be computed as [LHSV(h^{-1}) × (weight fraction hydrocarbon in the feed) × (feed density ($g\,cm^{-3}$))]/(catalyst bed density ($g\,cm^{-3}$)). Densities of the feed, 3 wt% Pt/Al_2O_3, and R-$Ni_{14}Sn$ were taken to be 1.0, 0.8, and 1.5 $g\,cm^{-3}$, respectively.

4.14 for R-$Ni_{14}Sn$. Interestingly, the H_2 uptake of R-$Ni_{14}Sn$ increased from 20.4 to 47.6 μmol $H_2\,g^{-1}$ after exposure to reaction conditions. These high CO:H uptake ratios are consistent with previous studies of NiSn alloys [12] and agree with the XRD and Mössbauer spectroscopic evidence that show the presence of NiSn alloys after reduction and reaction.

The BET surface area of the Raney-based catalysts slightly increased as a small amount of Sn was added to R-Ni, indicating improved thermal stability of R-$Ni_{270}Sn$ compared to R-Ni (Table 1). As more tin is added, however, the surface area slightly decreases. Thus, the addition of large amounts of Sn to R-Ni does not significantly decrease the surface area of the catalyst by pore blocking.

3.3. Reaction kinetics measurements

Aqueous-phase reforming of sorbitol, glycerol, and ethylene glycol solutions produces an effluent gas stream composed of 50–70 mol% H_2, 30–40 mol% CO_2, and 2–11 mol% alkanes (dry basis) at high conversion. Low concentrations of CO (less than 1000 ppm) were also detected in the outlet gas stream. The liquid effluent contained small amounts of unreacted feed, and trace amounts of byproducts, such as aldehydes, alcohols, and organic acids (less than 50 ppm at conversions greater than 90%) [3,4]. Analysis of the effluent gas and liquid streams yields a complete carbon balance for all feed molecules.

Selectivities for the production of H_2 and alkanes for the R-$Ni_{14}Sn$ and 3 wt% Pt/Al_2O_3 catalysts [1] are shown in Table 3 and Fig. 8. Over both catalysts, the selectivity for

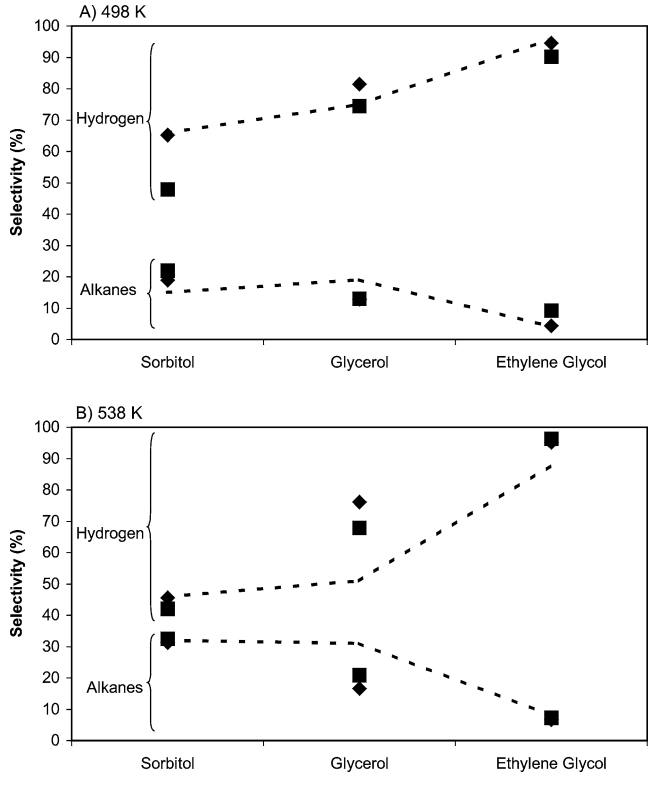

Fig. 8. Selectivity for production of hydrogen or alkanes by aqueous-phase reforming 1 wt% (◆) and 5 wt% (■) solutions of several oxygenated hydrocarbons over Raney $Ni_{14}Sn$ at (A) 498 K and 25.8 bar and (B) 538 K and 51.3 bar. The dotted lines represent previous results for reforming of 1 wt% feed solutions over Pt/Al_2O_3 at 498 K and 29.3 bar and 538 K and 56.0 bar, respectively [2].

production of H_2 decreases as the feed molecule becomes larger (i.e., ethylene glycerol > glycerol > sorbitol), while the selectivity for production of alkanes increases. As seen in Fig. 8, increasing the feed concentration from 1 to 5 wt% leads to lower H_2 and higher alkane selectivities for the R-Ni_{14}Sn catalyst. From Table 3 (or comparison of Fig. 8A and 8B) it appears that lower operating temperatures result in higher selectivities for production of H_2, which may be due in part to lower conversions of the feed molecules. It is important to note that the R-Ni_{14}Sn catalyst exhibits higher selectivity for production of H_2 and lower selectivity for production of alkanes than Pt/Al_2O_3 for reforming of glycerol and ethylene glycol solutions, while comparable selectivities are observed for reforming of sorbitol solutions. Table 3 also shows a difference in the distribution of alkanes produced, as the R-Ni_{14}Sn catalyst tends to produce more methane and smaller amounts of higher alkanes relative to Pt/Al_2O_3.

The effect on the H_2 and alkane selectivities of adding Sn to R-Ni catalysts can be seen in Table 4. As in high-throughput studies, the hydrogen selectivity improves from 35 to 51% at a Ni:Sn ratio of only 270:1, while alkane production is reduced more than 10% at 498 K. At a Ni:Sn ratio of 14:1, the hydrogen selectivity increases to 90%, while alkane production is nearly eliminated. These trends are even more dramatic for reforming at 538 K. Alkane formation appears to be primarily due to methanation of CO and/or CO_2, but some higher alkanes are produced by R-Ni and to a lesser extent over R-Ni_{270}Sn. Addition of tin raises the outlet CO concentration only at high temperature.

Addition of tin also alters the distribution of liquid phase products (Table 4). At 498 K, the selectivity to ethanol and acetaldehyde is significantly reduced and the selectivity to methanol is enhanced. At 538 K, addition of tin suppresses formation of acetic acid and promotes selectivity toward alcohols. Methanol may be produced either by direct hydrogenolysis of ethylene glycol or by series recombination of CO_2 and H_2. Methanol is a desirable product, since it still contains a C:O linkage and may be further reformed to produce H_2 in high yields [1,3]. Acetaldehyde is produced by dehydration of ethylene glycol, in which C:O linkages are replaced by alkane moieties, and the aldehyde can then be hydrogenated to form ethanol. These "alkane precursors" can be further dehydrated to form ethane. Acetic acid may be formed from isomerization of ethylene glycol, and it is especially troublesome due to its high stability in aqueous solution. Reforming of any of these alkane precursors cannot be carried out with high H_2 selectivity because methane is generated concurrently [4].

The total pressure of the system has a significant effect on the performance of Ni-based catalysts, as seen in Fig. 9. As the system pressure increases above the bubble point of the feed (25.1 bar at 498 K), production of alkanes increases and the hydrogen selectivity decreases accordingly. For example, aqueous-phase reforming over R-Ni_{14}Sn at a system pressure 0.5 bar above bubble-point leads to an alkane selectivity of less than 10% and a hydrogen selectivity of higher than

Table 4
Effect of Sn addition to Raney Ni 2800 catalysts for aqueous-phase reforming of 5 wt% ethylene glycol solutions

	Catalyst				
	R-Ni	R-Ni_{270}Sn	R-Ni_{14}Sn	R-Ni	R-Ni_{14}Sn
Temperature (K)	498	498	498	538	538
Pressure (bar)	25.8	25.8	25.8	51.3	51.3
LHSV (h^{-1})	4.13	2.76	2.57	8.26	10.3
H_2 selectivity (%)	35	51	90	28	96
Conversion of C to gas (%)	97	98	93	104	97
Alkane selectivity (%)	44	33	9	47	7
Gas products (mol%)					
H_2	47.6	56.5	69.3	41.4	70.7
CO_2	30.4	29.8	27.9	31.9	27.1
CO	0.02	0.03	0.03	0.03	0.10
Methane	20.7	12.9	2.65	25.6	1.98
Ethane	0.97	0.68	0.08	0.92	0.07
Propane	0.28	0.14	0.00	0.18	0.00
Butane	0.02	0.01	0.00	0.01	0.00
Liquid products (mol%, excluding unreacted EG)					
Methanol	10.2	67.7	52.9	34.3	76.9
Ethanol	48.3	19.0	11.1	2.5	20.7
Acetic acid	30.2	13.4	35.9	63.2	2.2
Acetaldehyde	7.3	0.0	0.0	0.0	0.2
Glycolaldehyde	4.0	0.0	0.0	0.0	0.0
Liquid C as by-products[a]	6.3	5.2	24.2	17.2	99.3

[a] Defined as (moles of carbon as liquid by-products)/(total moles of carbon in the liquid products) ×100%.

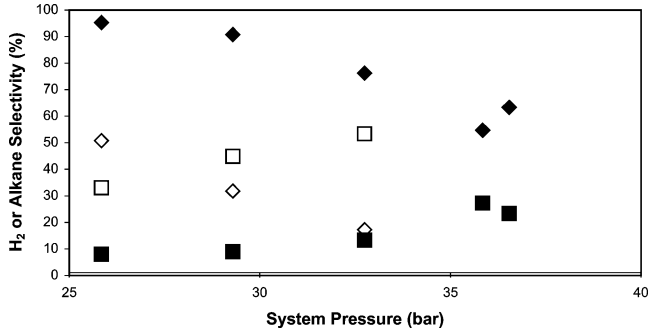

Fig. 9. Effect of system pressure on the hydrogen (◆) and alkane (■) selectivities for aqueous-phase reforming of 5 wt% ethylene glycol solutions at 498 K over R-Ni_{14}Sn (solid symbols) and R-Ni_{270}Sn (hollow symbols).

90%, whereas the alkane selectivity increases to nearly 30% and the hydrogen selectivity decreases to 60% at a system pressure of 37 bar. The activity of the catalyst also decreases as the pressure rises, leading to lower conversions. This loss of activity has been associated with inhibition by high product partial pressures and reactor dynamics in studies of Pt catalysts [3,5].

Fig. 10 shows that the hydrogen selectivity is also affected by the space velocity through the reactor. At sufficiently high space velocities (i.e., short residence times), the hydrogen selectivity approaches a different maximum value for each feed molecule. As the space velocity decreases (i.e., longer residence times), the hydrogen selectivity decreases due to methane formation from CO_2 and H_2.

Table 5
Rates of formation of various products by aqueous-phase reforming of 5 wt% ethylene glycol at 498 K and 25.8 bar

Catalyst	LHSV (h^{-1})	Conversion % C to gas	H_2 selectivity (%)	Alkane selectivity (%)	TOF (min^{-1})							H_2 production ($\mu mol\,cm^{-3}$ reactor min^{-1})
					H_2	CO_2	CO	CH_4	C_2H_6	C_3H_8	Total C	
Raney Ni	85.9	13.7	46.9	33.1	1.1	0.61	0.0243	0.278	0.0142	0.0028	0.95	366
Raney $Ni_{270}Sn$	34.7	32.6	57.1	26.8	1.4	0.69	0.0303	0.231	0.0129	0.0022	0.99	431
Raney $Ni_{14}Sn$	42.1	13.2	93.2	5.3	1.4	0.55	0.0043	0.031	0	0	0.59	355
Raney Ni_4Sn	26.6	4.9	118.9	0	1.2	0.41	0.0048	0	0	0	0.41	104
Pt/Al_2O_3	129	5.4	97.9	0	5.3	2.2	0.0051	0	0	0	2.2	449

Metal dispersions are listed in Table 2, and bed densities of 0.8 and 1.5 $g\,cm^{-3}$ are used for the Pt/Al_2O_3 and Raney Ni-based catalysts, respectively. Rates were measured after 6 h time on stream and based on irreversible CO uptake.

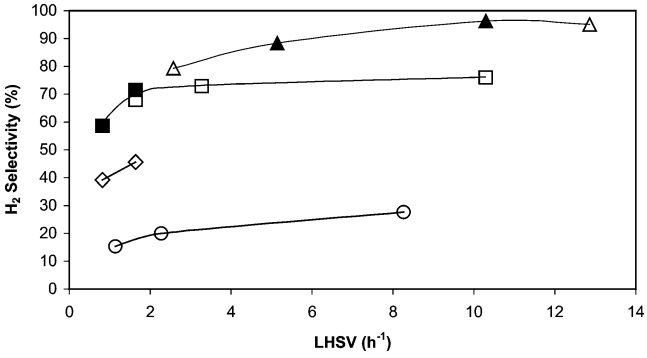

Fig. 10. Hydrogen selectivity as a function of space velocity for aqueous-phase reforming of sorbitol (◆), glycerol (■), and ethylene glycol (▲) solutions at 538 K and 51.3 bar over R-$Ni_{14}Sn$, and aqueous-phase reforming of ethylene glycol (●) solutions at 538 K and 51.3 bar over R-Ni. Conversion is above 89% for all points. Hollow symbols denote a feed concentration of 1 wt%, while solid symbols correspond to 5 wt% feed.

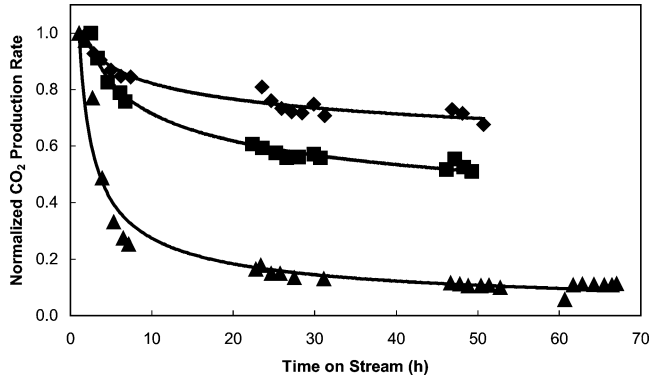

Fig. 11. Deactivation profiles for Raney $Ni_{14}Sn$ (◆), Raney Ni 2800 (■), and Ni_9Sn/Al_2O_3 (▲) during aqueous-phase reforming of 10 wt% ethylene glycol solutions at 498 K and 29.3 bar. Values of CO_2 production rate are normalized by the initial activity (CO_2 TOF of 0.45, 0.66, and 0.26 min^{-1}, respectively). Final conversions are 7–10%.

These observations suggest that alkane production by Ni-based catalysts occurs both by dehydration/hydrogenation (i.e., through C–O bond cleavage and alkane precursors) and by series recombination of the product CO and CO_2 with H_2 (i.e., through methanation or Fischer–Tropsch synthesis).

Table 5 shows reaction kinetics data for aqueous-phase reforming of ethylene glycol solutions at conversions lower than 30%. Similar to the behavior observed at high conversions, addition of Sn to Raney Ni catalysts decreases alkane production and improves the hydrogen selectivity at low conversions. For example, R-$Ni_{14}Sn$ produces 10 times less methane (H_2 selectivity of 93%) compared to unpromoted R-Ni (H_2 selectivity of 47%), and addition of Sn completely eliminates propane and butane formation by Fischer–Tropsch synthesis. Addition of tin decreases the overall rate of ethylene glycol consumption by selectively reducing alkane formation, since H_2 rates are nearly unaffected and CO_2 rates decrease only slightly even for R-Ni_4Sn. Also, addition of moderate amounts of Sn slows the rate of CO production. Addition of large amounts of Sn reduces the reforming activity, as seen for R-Ni_4Sn, for which low conversion leads to artificially high hydrogen selectivity.

We note that turnover frequencies for hydrogen production at 498 K over the Raney-Ni-based catalysts are similar to each other and lower than that over 3 wt% Pt/Al_2O_3 (based on the extents of CO adsorption). However, the high CO uptakes and high densities of the Raney-Ni-based catalysts lead to comparable rates of hydrogen production per unit reactor volume as for 3 wt% Pt/Al_2O_3. Furthermore, since addition of Sn significantly decreases the extent of H_2 adsorption, the turnover frequency for hydrogen production based on H uptake is enhanced over Raney-NiSn, such that R-$Ni_{14}Sn$ has higher catalytic activity than Pt/Al_2O_3 on this basis. We also conclude that these data are not likely to be controlled by transport limitations, because previous experiments show that the Pt/Al_2O_3 catalyst operates in the kinetic regime under these conditions [3], and rates per reactor volume are similar for the R-Ni-based catalysts as for Pt/Al_2O_3.

3.4. Catalyst deactivation

Raney-Ni-based catalysts display relatively stable performance versus time on stream for aqueous-phase reforming, as seen in Fig. 11. However, it is apparent in this figure that alumina-supported nickel catalysts exhibit severe deactivation phenomena. For example, catalysts comprised of Ni supported on Al_2O_3, SiO_2, and ZrO_2 lost 90% of their initial activity over a period of 2 days, and subsequent calcination at 573 K in flowing O_2 followed by reduction at 523 K in H_2 did not restore catalytic activity. X-ray diffraction patterns

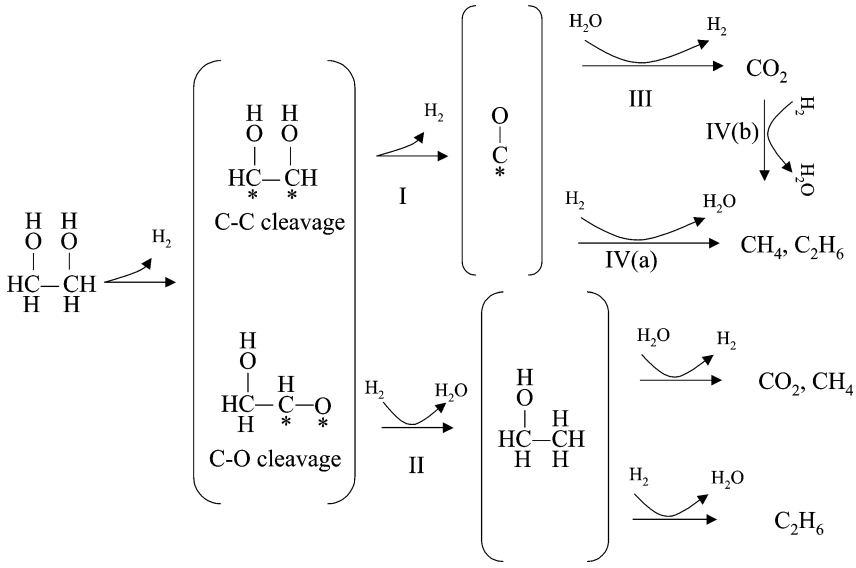

Fig. 12. Schematic representation of reaction pathways and selectivity challenges for production of H_2 from conversion of ethylene glycol with water. Pathway I is desired C–C cleavage to form adsorbed CO. Pathway II represents undesired C–O cleavage followed by hydrogenation to produce ethanol, leading to formation of methane and ethane. Pathway III is the desired water–gas-shift reaction. Pathway IV represents undesired methanation and Fischer–Tropsch reactions to produce alkanes.

of the reduced, fresh, and spent alumina-supported catalysts show significant narrowing of the diffraction peaks, indicating an increase in the Ni particle size from 7 to 125 nm according to the Scherrer equation. This behavior is consistent with the severe loss of CO uptake observed after exposure to reaction conditions (Table 1). Sintering of Ni catalysts has been previously reported in high-pressure aqueous environments, but a proprietary Ni catalyst is known to be stable under significantly harsher, supercritical conditions (623 K and 200 bar) [13].

It is apparent from Fig. 11 that addition of Sn to the Raney-Ni catalyst further improves catalyst stability during aqueous-phase reforming. The rate of H_2 production over R-Ni_{14}Sn decreased by only 15% after 10 h (compared to 25% decrease for R-Ni) and reached a constant value equal to 72% of the initial activity after 48 h. We also tested the catalyst at high conversion for over 340 h without regeneration. The initial decrease in catalytic activity is consistent with the similar decrease in the extent of CO chemisorption by the catalyst from 168 to 140 $\mu mol\, g^{-1}$ after exposure to reaction conditions for 48 h, which may be due to sintering of the catalyst. Deactivation due to leaching of Ni and Sn from this R-Ni_{14}Sn catalyst is minimal under high conversion conditions (about 1 and 5 wppm Sn and Ni were detected in the liquid reactor effluent). However, leaching by acid by-products formed at low conversions may be possible.

4. Discussion

Reaction pathways and selectivity challenges for production of H_2 by aqueous-phase reforming of ethylene glycol are outlined in Fig. 12. Adsorbed ethylene glycol may undergo desired C–C cleavage to form adsorbed CO and H_2 (Pathway I) or undesired C–O cleavage (Pathway II) to produce ethanol, methane, and ethane after reaction with H_2. Adsorbed CO may be consumed by the desired water–gas-shift reaction (Pathway III) to give CO_2 and H_2 or form alkanes by undesired methanation and Fischer–Tropsch reactions (Pathway IV). Nickel catalysts are promising for the APR process because they readily cleave C–C bonds [14] and show high activity for the water–gas-shift reaction [15]. However, nickel catalysts also cleave C–O bonds, especially in the hydrogenation of CO and CO_2 (through the reverse water–gas-shift reaction) to form methane [16–20].

Oxygenated hydrocarbons readily undergo hydrogenolysis reactions on Ni surfaces. For example, cleavage of C–H and C–C bonds has been observed to take place at temperatures below 500 K in reactions of ethanol and acetaldehyde on Ni single crystals [21]. Such behavior has also been observed in reactions of ethanol over Pt/SiO_2 in excess H_2 that lead to hydrogenolysis products CO and CH_4 at temperatures near 500 K [22]. Theoretical studies, using DFT calculations on Pt, show that the rate of C–C bond cleavage in an oxygenated hydrocarbon such as ethanol is faster than the rate of C–C bond cleavage in an alkane such as ethane [23]. Importantly, the addition of Sn to Ni catalysts has been shown to decrease the rates of alkane hydrogenolysis reactions and to enhance the selectivity to dehydrogenated products [24]. The primary effect of adding Sn to Ni must be the suppression of C–O bond cleavage and methanation reactions, while maintaining sufficient catalytic activity for cleavage of C–C bonds.

The beneficial effect we have observed by adding Sn to Ni on the selectivity for the production of hydrogen may be

caused by the presence of Sn at Ni-defect sites and by the formation of Ni–Sn alloy surfaces, such as a Ni_3Sn alloy. In this respect, dissociation of CO leading to formation of methane over Ni may take place preferentially on Ni-defect sites [25], analogous to the preferential dissociation of dinitrogen on Ru-defect sites [26]. Accordingly, the decoration of defect sites by Sn may suppress methanation reactions, analogous to the observation that decoration of Ru-defect sites by Au decreases the rate of N_2 dissociation at 500 K by seven orders of magnitude [26]. It is also possible that methanation reactions are suppressed by geometric effects caused by the presence of Sn on Ni–Sn alloy surfaces, i.e., by decreasing the number of surface ensembles composed of multiple nickel atoms that are necessary for CO or H_2 dissociation.

Adsorption of CO on Ni(111) is known to be favored at threefold-hollow sites [27]. Our observation that addition of Sn to R-Ni causes a decrease in the CO uptake is consistent with the report that adsorption of CO is strongly suppressed on a buckled $(\sqrt{3} \times \sqrt{3})R30^\circ$ Sn/Ni(111) surface which has no threefold Ni hollow sites [28]. The suppression of CO adsorption by addition of Sn to Ni may be analogous to the weakening of CO adsorption on Cu surfaces caused by Zn and ZnO species [29]. Weaker adsorption of CO and H atoms may alleviate poisoning of the catalyst by high surface coverages of these reaction intermediates. Cleavage of C–O bonds may also be slowed on Sn-promoted Ni surfaces by electronic effects, because Sn has been reported to weaken the adsorption of carbide fragments (coke) that are known to be intermediates in the production of methane [24].

Our reaction kinetics measurements are consistent with a previous study by Velu et al. [30] of the vapor-phase decomposition and steam reforming of methanol over Sn-promoted NiAl catalysts. Over the unpromoted Ni catalyst, methanol decomposition to carbon monoxide and hydrogen was favored at low temperatures (473 K) and low conversions ($\sim 5\%$). At higher temperatures, decomposition was accompanied by water–gas shift to form CO_2 from a small fraction of the CO, and nearly all of the hydrogen was consumed to produce methane. In contrast, the Sn-promoted catalyst showed high selectivity toward formation of H_2 and CO over the entire temperature range tested.

Our characterization studies of Ni–Sn catalysts (e.g., XRD, Mössbauer spectroscopy) suggest that Sn migrates into the Ni particles to form Ni–Sn alloys. Masai and coworkers [31] prepared silica-supported Ni_1Sn_1 and $Ni_{2.5}Sn_1$ catalysts by surface reaction of tetrabutyl tin with Ni/SiO_2, and they detected Ni_3Sn_4, Ni_3Sn_2, NiSn, and β-tin phases after reduction in H_2 at 773 K, whereas Ni_3Sn_4, NiSn, and Ni were present in a $Ni_{10}Sn_1/SiO_2$ catalyst. They speculate that molten tin diffuses into the Ni crystallites during high-temperature reduction, forming NiSn alloys. Indeed, diffusion of Sn into Ni occurs rapidly at elevated temperature, especially above the melting point of Sn (505 K). Bulk diffusivities have been reported as high as 4.2×10^{-18} and 4.9×10^{-13} $m^2\,s^{-1}$ at 453 and 553 K, respectively, for the Ni–Sn system [32].

Onda and co-workers [33] studied the extent of alloying between nickel and tin in silica-supported catalysts prepared by chemical vapor deposition of $Sn(CH_3)_4$ onto Ni/SiO_2. They found that temperatures of 448–498 K were sufficient not only to deposit tin on the Ni particles, but also to begin diffusion of tin into nickel. These authors used temperature-programmed reduction (TPR) [33] to show that Ni–Sn compounds reduce at lower temperatures than Sn alone. For example, while Sn/SiO_2 reduces at temperatures above 800 K, Ni_3Sn_4/SiO_2 catalysts reduce near 650 K, nickel-rich catalysts begin to form between 450 and 500 K, and Ni/SiO_2 reduces near 400 K. These results agree well with TPR data for unsupported alloys [34].

It appears from the literature that formation of Ni–Sn alloys can be hindered by calcination pretreatment of the catalysts. Arana et al. [35] found that reduction of fresh catalysts formed Ni_3Sn_2 after 1 h at 673 K, while Onda required 1 h at 723 K and an additional hour at 873 K to form Ni_3Sn_2 in a calcined sample. Subsequent calcination of the reduced Ni_3Sn_2/SiO_2 formed by Arana et al. for 2 h at 673 K led to decomposition of some of the alloy to form Ni_3Sn and SnO_2 (as opposed to formation of NiO for Ni/SiO_2 catalysts under these conditions). Our Mössbauer spectroscopic results also indicate that slight oxidation of the Ni_3Sn alloy occurred during exposure to aqueous-phase reforming reaction conditions at 498 K.

We observed in the present study that addition of Sn to Raney Ni catalysts improves the stability of the catalyst under aqueous-phase reforming conditions. This behavior is consistent with the fact that Sn can be added to Ni surfaces to improve corrosion resistance [36].

The key difference between aqueous-phase reforming over Ni-based and Pt-based catalysts is that over Ni-based catalysts CO and CO_2 react with H_2 to form methane, while slow methane production occurs over supported Pt catalysts by dehydration/hydrogenation and subsequent C–C bond cleavage [4]. Although addition of Sn to Ni catalysts greatly reduces the rate of methane formation, to achieve the highest selectivities for production of H_2 it is also essential to minimize the partial pressures of the product gases and their residence time in the reactor. We have shown previously that operation of the reactor near the bubble point of the feed solution can be used to reduce the partial pressures of product gases in the reactor due to dilution by water vapor [3,5]. Accordingly, lower system pressures (Fig. 9) and/or shorter reactor space times (Fig. 10) lead to decreases in alkane formation over R-NiSn catalysts by minimizing methanation and Fischer–Tropsch processes. Thus, it is possible to achieve high hydrogen selectivities at pressures near the bubble point of the feed and at moderate reactor space times over R-NiSn catalysts, while it is impossible to achieve these high selectivities under any conditions over unpromoted R-Ni catalysts. Catalysts based on Pt can be used effectively for

hydrogen production over a wider range of operating conditions, since they suffer less from series selectivity issues.

5. Conclusions

A R-NiSn catalyst can be used to achieve good activity, selectivity, and stability for production of hydrogen by aqueous-phase reforming of biomass-derived oxygenated hydrocarbons. This inexpensive material has catalytic properties that are comparable to those of Pt/Al_2O_3 for production of hydrogen from small oxygenates, such as ethylene glycol, glycerol, and sorbitol. Rates of hydrogen production by aqueous-phase reforming of ethylene glycol over R-NiSn catalysts with Ni:Sn atomic ratios of up to 14:1 are comparable to 3 wt% Pt/Al_2O_3, based on reactor volume or H_2 chemisorption uptake.

The addition of Sn to Raney Ni catalysts significantly reduces the rate of methane formation from series recombination of CO or CO_2 with H_2, while maintaining high rates of C–C cleavage necessary for production of H_2. However, it is necessary to operate the reactor near the bubble-point pressure of the feed and moderate space times to achieve high selectivities for production of H_2 over R-NiSn catalysts, while it is impossible to achieve these high selectivities under any conditions over unpromoted R-Ni catalysts. The Sn-promoted Raney-Ni catalyst is catalytically stable for more than 340 h time on stream at high conversion.

Characterization of the R-NiSn catalysts by XPS, XRD, and Mössbauer spectroscopy shows that Sn migrates into Ni particles to form a Ni_3Sn phase around a core of Ni after reduction in hydrogen and exposure to reaction conditions. The high selectivity of R-NiSn catalysts for production of hydrogen may be related to the presence of Ni_3Sn, or Sn may selectively poison Ni-defect or edge sites that may be responsible for methanation of CO or CO_2. Addition of Sn to Ni catalysts significantly decreases adsorption uptakes by CO and H_2, with a more significant effect on the adsorption of H_2. It is likely that recent advances in the understanding of heterogeneous catalysis [37,38], combined with advances in the synthesis and in situ characterization of new catalytic materials [39,40], will lead to new generations of catalysts, probably based on metal alloys, for the environmentally sustainable production of hydrogen by aqueous-phase reforming of biomass-derived oxygenated hydrocarbons.

Acknowledgments

This work was supported by U.S. Department of Energy (DOE), Office of Basic Energy Sciences, Chemical Sciences Division. We also acknowledge funding from the Energy Center of Wisconsin and the University of Wisconsin Office of University-Industrial Relations. We thank Won Bai Kim for assistance in catalyst characterization.

References

[1] R.D. Cortright, R.R. Davda, J.A. Dumesic, Nature 418 (2002) 64.
[2] R.R. Davda, J.W. Shabaker, G.W. Huber, R.D. Cortright, J.A. Dumesic, Appl. Catal. B 43 (2002) 13.
[3] J.W. Shabaker, G.W. Huber, R.R. Davda, R.D. Cortright, J.A. Dumesic, J. Catal. 215 (2003) 344.
[4] J.W. Shabaker, G.W. Huber, R.R. Davda, R.D. Cortright, J.A. Dumesic, Catal. Lett. 88 (2003) 1.
[5] R.R. Davda, J.A. Dumesic, Ang. Chem., Int. Ed. 42 (2003) 4068.
[6] G.W. Huber, J.W. Shabaker, J.A. Dumesic, Science 300 (2003) 2075.
[7] G.E. Moulder, W.F. Stickle, P.E. Sobol, K.D. Bomben, Handbook of X-Ray Photoelectron Spectroscopy, 2nd ed., Perkin-Elmer, Physical Electronics Division, Wellesley, MA, 1992.
[8] S.D. Robertson, J. Freel, R.B. Anderson, J. Catal. 24 (1972) 130.
[9] R. Mildenberger, A. Venskutonis, F. Aubertin, J. Breme, G. Schwitzgebel, Hyperfine Interact. 112 (1998) 151.
[10] P. Nash, A. Nash, Bull. Alloy Phase Diag. 6 (1985) 350.
[11] C.H. Bartholomew, R.B. Pannel, J. Catal. 65 (1980) 390.
[12] M. Agnelli, J.P. Candy, J.M. Basset, J.P. Bournonville, O.A. Ferretti, J. Catal. 121 (1990) 236.
[13] D.C. Elliot, L.J. Sealock, E.G. Baker, Ind. Eng. Chem. Res. 32 (1993) 1542.
[14] J.H. Sinfelt, D.J.C. Yates, J. Catal. 8 (1967) 82.
[15] D.C. Grenoble, M.M. Estadt, D.F. Ollis, J. Catal. 67 (1981) 90.
[16] J. Wambach, A. Baiker, A. Wokaun, Phys. Chem. Chem. Phys. 1 (1999) 5071.
[17] J. Happel, I. Suzuki, P. Kokayeff, V. Fthenakis, J. Catal. 65 (1980) 59.
[18] J. Happel, H.Y. Cheh, M. Otarod, S. Ozawa, A.J. Severdia, T. Yoshida, V. Fthenakis, J. Catal. 75 (1983) 314.
[19] D.W. Goodman, R.D. Kelley, T.E. Madey, J.T.J. Yates, J. Catal. 63 (1980) 226.
[20] S.Z. Ozdogan, P.D. Gochis, J.L. Falconer, J. Catal. 83 (1983) 257.
[21] S.M. Gates, J.N. Russel, J.T.J. Yates, Surf. Sci. 171 (1986) 111.
[22] K. Gursahani, R. Alcala, R.D. Cortright, J.A. Dumesic, Appl. Catal. A 222 (2001) 369.
[23] R.R. Davda, R. Alcala, J.W. Shabaker, G. Huber, R.D. Cortright, M. Mavrikakis, J.A. Dumesic, in: Fourth Tokyo Conference on Advanced Catalytic Science and Technology, Tokyo, Japan, 2002.
[24] A.D. Logan, M.T. Paffett, in: 10th International Congress on Catalysis, Budapest, Hungary, 1992.
[25] H.P. Steinruck, M.P. D'evelyn, R.J. Madix, Surf. Sci. 172 (1986) L561.
[26] S. Dahl, A. Logadottir, R.C. Egeberg, J.H. Larsen, I. Chorkendorff, E. Törnqvist, J.K. Nørskov, Phys. Rev. Lett. 83 (1999) 1814.
[27] L. Becker, S. Aminpirooz, B. Hillert, M. Pedio, J. Haase, D.L. Adams, Phys. Rev. B 47 (1993) 9710.
[28] C. Xu, B.E. Koel, Surf. Sci. 327 (1995) 38.
[29] J. Greeley, A.A. Gokhale, J. Kreuser, H. Topsøe, N.-Y. Topsøe, M. Mavrikakis, J.A. Dumesic, J. Catal. 213 (2003) 63.
[30] S. Velu, K. Suzuki, T. Osaki, Catal. Lett. 69 (2000) 43.
[31] M. Masai, K. Mori, H. Muramoto, T. Fujiwara, S. Ohnaka, J. Catal. 38 (1975) 128.
[32] T. Ozawa, A. Maeda, T. Itoh, T. Umemura, Microjoining and Assembly Technology in Electronics, Sagamihara, Kanagawa, Japan, 2002.
[33] A. Onda, T. Komatsu, T. Yashima, J. Catal. 201 (2001) 13.
[34] A. Onda, T. Komatsu, T. Yashima, Chem. Commun. 15 (1998) 1507.
[35] J. Arana, P.R. d. l. Piscina, J. Llorca, J. Sales, N. Homs, J.L.G. Fierro, Chem. Mater. 10 (1998) 1333.
[36] S.C. Britton, R.M. Angles, J. Electrodepositors' Tech. Soc. 27 (1951) 293.
[37] J. Greeley, J.K. Nørskov, M. Mavrikakis, Annu. Rev. Phys. Chem. 53 (2002) 319.
[38] F. Besenbacher, I. Chorkendorff, B.S. Clausen, B. Hammer, A.M. Molenbroek, J.K. Norskov, I. Stensgaard, Science 279 (1998) 1913.
[39] P.L. Hansen, J.B. Wagner, S. Helveg, J.R. Rostrup-Nielsen, B.S. Clausen, H. Topsoe, Science 295 (2002) 2053.
[40] A.T. Bell, Science 299 (2003) 1688.